ACS APPLIED MATERIALS & INTERFACES

Research Article

www.acsami.org

Novel Transparent Zirconium-Based Hybrid Material With Multilayered Nanostructures: Studies of Surface Dewettability Toward Alkane Liquids

Benjamin Masheder, Chihiro Urata, Dalton F. Cheng, and Atsushi Hozumi*

National Institute for Advanced Industrial Science and Technology (AIST) 2266-98, Anagahora, Shimo-Shidami, Moriyama-ku Nagoya, Aichi 463-8560, Japan

Supporting Information

ABSTRACT: We have successfully prepared unique inorganic−organic hybrid materials that demonstrate excellent transparency and dewettability toward various alkane liquids (*n*-hexadecane, *n*-dodecane and *n*-decane) without relying on conventional surface roughening and perfluorination. Such coatings were made using a novel family of hybrid materials generated by substituting carboxylic acids, with a range of alkyl chain lengths ($CH_3(CH_2)_{x-2}COOH$ where x = total carbon number, i.e., 10, 12, 14, 16, 18, 22, or 24, into zirconium (Zr) tetra-propoxide complexes. This precursor was then mixed with acetic acid and spincast to produce transparent thin Zr-carboxylic acid ($ZrCA_x$) hybrid films using a nonhydrolytic sol−gel process. Fourier transform infrared spectroscopy provided proof of Zr−O−Zr network formation in the films upon casting and also followed changes to the physical nature (liquid-like or solid-like) of the alkyl chain assemblies depending upon alkyl chain length. X-ray diffractometry revealed that the hybrid films prepared using the longer chain carboxylic acids ($ZrCA_{x\geq 18}$) spontaneously self-assembled into lamella structures with *d*-spacings ranging from 29.5 to 32.7 Angstroms, depending on the length of the alkyl chain. On the other hand the remaining films ($ZrCA_{x<18}$) showed no such ordering. Moreover, the dynamic dewetting behavior of our hybrid films with alkane liquids was also strongly affected by alkyl chain length. $ZrCA_x$ films with x = 12, 14, and 16 showed the best dynamic oleophobicity among the seven hybrid films. In particular, small volume alkane droplets (5 μL) could be easily set in motion to move across and off $ZrCA_{14}$ film surfaces without pinning at low tilt angles (~6°).

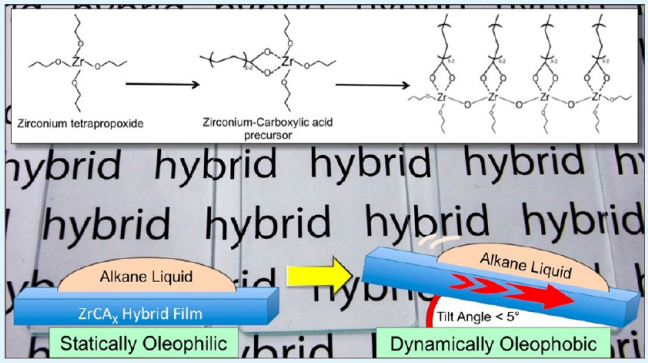

KEYWORDS: *zirconium-based hybrid, lamella structure, carboxylic acid, dynamic dewettability, oleophobicity*

INTRODUCTION

Coatings that easily dewet liquids from their surfaces have many varied and useful applications including providing self-cleaning properties, corrosion protection, and in the production of food packaging and antifingerprint displays.[1−8] The purpose of such materials is to prevent liquid droplets from adhering or pinning to a surface and consequently allowing easy dewetting, for instance permitting even a small droplet to slide across and off a slightly inclined surface as a result of gravity alone. Traditionally, the design of easy-dewetting surfaces has focused on producing surfaces with an extremely high (≥150°) static contact angle (CA), with such surfaces commonly classified as "superhydrophobic" or "superoleophobic", for aqueous or organic liquids respectively.[9] The preoccupation with creating surfaces which have high static CAs might be attributable to the frequent citation of lotus leaves or water strider's leg as model examples of superhydrophobic surfaces which easily dewet water.[3,10−12] The repeated referral to these and other natural superhydrophobic surfaces as archetypes of easy-dewetting materials perhaps led to the presumption that if a surface exhibits a smaller liquid−solid contact area than another surface, it will therefore require a smaller tilt angle (TA) to facilitate droplet dewetting. However, CA hysteresis has recently been cited as a better method of judging the dewettability of a surface (where CA hysteresis ($\Delta\theta$) = advancing CA (θ_A) − receding CA (θ_R) or $\Delta\theta_{cos} = \cos\theta_R - \cos\theta_A$).[13−16]

$$F = mg\sin\alpha = kw\gamma_{LV}(\cos\theta_R - \cos\theta_A) \quad (1)$$

Equation 1 describes the gravitational force required to initiate drop movement across a tilted solid surface as being dependent on CA hysteresis, where m is the mass of the drop, g is the gravitational constant, α is the substrate TA, k is a constant that depends on drop shape, w is the width of the drop, and γ_{LV} is the liquid−vapor surface tension. An easy-dewetting surface will therefore have a very low CA hysteresis and TA (<10°) for a

Received: October 14, 2012
Accepted: December 10, 2012
Published: December 10, 2012

small volume droplet (3−10 μL), jointly termed dynamic dewettability.

Although the creation of superhydrophobic surfaces has received widespread attention and credible success,[17−20] the production of superoleophobic surfaces has proven significantly more difficult and challenging, in part because of the very low surface tension of some alkane liquids. The construction of superoleophobic surfaces has typically followed a very similar approach to that of their superhydrophobic counterparts, often employing both engineered surface micro/nanostructures and subsequent surface perfluorination to induce high static CAs.[9] These two features are used to promote the creation of a Cassie state for the droplet,[2,21−23] and to lower the surface energy of the material[24] respectively, which collectively decreases the overall solid−liquid interaction. Although fairly successful, there are a number of drawbacks to this approach. For instance, the use of prominent topographical features on a surface typically yields inferior robustness, low transparency, a susceptibility for droplet pinning to occur, and poor dewettability for low surface tension liquids.[2,9,25] There have also been concerns raised about the effects of long-chain perfluorinated compounds (LCPFCs) on human health and the environment. For instance, some LCPFCs commonly used in dewettable surfaces have been recently listed as persistent organic pollutants.[26−28] In response to these shortcomings, calls have been made for new surfaces showing highly dewetting properties toward alkane liquids without relying on such conventional physical and chemical treatments.

In contrast to such topographically modified (high static CA) surfaces, there have only been a few reports of flat/smooth surfaces showing low CA hysteresis and TAs against alkane liquids. Such surfaces typically possess a similar physical nature (liquidlike) generated by the use of the specific molecular structures (branched[29,30] or ring-shaped molecules[31]) or reduced packing density through shortened reaction times.[32] All of which produce excellent dynamic dewetting behavior, allowing alkane liquid droplets to easily dewet from the surface at low TAs, independent of the CA magnitude. Liquid-like surface properties typically arise when surface-tethered functional groups have a high degree of freedom to move and be flexible, allowing probe droplets in contact with them to experience very low energy barriers between metastable states, resulting in the formation of low CA hysteresis surfaces.[33] McCarthy's group reported that silicon surfaces treated with various silanizing agents, such as $Cl(SiMe_2O)_nSiMe_2Cl$ (n = 0−3), $(Me_3SiO)_3SiCH_2CH_2Si(Me)_2Cl$, and $(Me_3SiO)_2SiMeCH_2CH_2Si(Me)_2Cl$, showed low static CAs and $\Delta\theta$ (1−4°) for n-hexadecane (θ_A/θ_R = ∼36°/∼35°, ∼38°/∼36°, and ∼30°/∼26°, respectively).[29] We have since reported that low $\Delta\theta$ (2−3°) surfaces for n-hexadecane (θ_A/θ_R = ∼31−33°/∼28−31°) could also be prepared using monolayers consisting of cyclic organosilanes not only on silicon substrates but also on other substrates, including oxidized aluminum and titanium.[31] Besides these monolayer-covered surfaces, it has been reported that alkylmethyldichlorosilanes ($RMeSiCl_2$, where R = CH_3, C_4H_9, and C_6H_{13}) formed oligomeric layers on silicon substrates from the vapor phase and exhibited low static CAs and $\Delta\theta$ for n-hexadecane (θ_A/θ_R = 36°/34°, 18°/14°, and 15°/10°, respectively).[34] The use of polymer brush films for the purpose of controlling the dynamic dewettability has also been identified very recently. Krumpfer et al. reported that $\Delta\theta$ for n-hexadecane was small (2−6°) for thin poly(dimethylsiloxane) (PDMS) brush films consisting of very low molecular weight (MW) polymers (MW 2000).[35] In this case, dynamic CA values for n-hexadecane depended on the preparation conditions and substrates, and were typically θ_A/θ_R = ∼35−37°/∼29−35°. The authors then prepared a series of PDMS brush films with different MWs.[36,37] These surfaces were all smooth and nonperfluorinated and exhibited excellent dynamic dewettability, while also displaying an oleophilic nature. For instance, a 3 μL droplet of n-decane has been shown to totally dewet a smooth PDMS brush surface with low CA hysteresis (MW 6000, θ_A/θ_R = 14.1°/14°, static CA of 14°) at a TA of only 1° above horizontal. Such an extremely low TA for small volume droplets of alkane liquids, to the best of the author's knowledge, has not been realized by any perfluorinated or superoleophobic surfaces. This is clear evidence that beneficial interactions between the probe liquid and the surface are more practically important than the maximum achievable static CA. In this case, we expect that the surface tethered PDMS chains interact with polar and nonpolar alkane liquids in a very different way, repelling polar liquids while becoming reversibly solvated and swollen by nonpolar alkane liquids. The mutual affinity of the alkane liquids and the PDMS chains causes the formation of a "blended liquid−liquid interface" containing a highly fluid layer of PDMS chains. This alters the physical nature of the surface because of the relatively high mobility of the swollen polymer chains when compared to nonswollen PDMS brush films, resulting in excellent dynamic dewettability for alkane liquids. Alternatively, polar liquids like water experience mutual hydrophobic repulsion at the surface and a distinctly liquid−solid interaction, producing higher static CAs in addition to higher $\Delta\theta$ and TAs than nonpolar liquids. The underlying importance of these findings was that instead of using textured surfaces and perfluorinated compounds designed to increase the repulsion between a surface and a liquid, it is possible to get exceptional dewettability by enhancing the mutual interaction.

In spite of such monolayer- or polymer-covered surfaces offering excellent dynamic dewetting behavior, there are however requirements for further improvement to the mechanical properties of these approaches, such as hardness and durability, before widespread use becomes practical. For example, these films are generally very thin (<3 nm), therefore surface dewettability is markedly influenced by substrate surface morphology.[38] Consequently, highly dewettable films with transparency and sufficient thicknesses so as to remove the need for substrate flatness control are greatly required. To address these challenges, sol−gel based inorganic−organic hybrid films have recently been found to satisfy many of the required qualities, especially the well-documented Si-organic family of materials. Such hybrid films have provided highly transparent and smooth surfaces, regardless of the flatness of the substrate due to the thickness of the coatings (>500 nm), with reasonable adhesive properties to the underlying substrate.[39,40] Unfortunately, with the exception of our recent report,[39] the use of such sol−gel hybrid coatings for the purpose of controlling dynamic hydrophobicity/oleophobicity has been rarely seen. In particular, fundamental studies of surface wetting/dewetting properties of other inorganic−organic sol−gel hybrid systems have not been reported in detail. Thus, the authors paid attention to zirconium (Zr)-based hybrid materials because they are one of the most widely employed protective materials, notably zirconia (ZrO_2) or yttria-stabilized zirconia (YSZ) ceramics which are well renowned for their high hardness and durability to wear and

chemical attack. However, such oxide surfaces are generally hydrophilic, oleophilic and possess poor dewettability.[41] The materials presented for the first time in this article are smooth, transparent Zr-organic hybrid films that demonstrate excellent dynamic dewetting behavior for various low surface tension alkane liquids. Previous common uses of Zr-based hybrid materials have predominantly been limited to use as precursors in the production of mesoporous ZrO_2 through hydration and subsequent elimination of the organic content by calcination.[42] In this study, we used anhydrous, noncalcined Zr-based inorganic−organic hybrids to provide highly dewettable, smooth, and transparent films.

Acetate addition to ZTP:

$$\underset{(ZTP)}{Zr(OR)_4} + \underset{(AA)}{CH_3COOH} \rightarrow \underset{(ZTP-AA)}{Zr(OR)_3(CH_3COO^-)} + ROH(R = (CH_2)_2CH_3) \quad (2)$$

Hydrolysis:

$$Zr(OR)_4 + nH_2O \rightarrow Zr(OR)_{4-n}(OH)_n + nROH \quad (3)$$

Acetate addition to $ZrCA_x$:

$$\underset{(ZrCA_x)}{Zr(OR)_3(CH_3(CH_2)_{x-2}COO^-)} + \underset{(AA)}{CH_3COOH} \rightarrow \underset{(ZrCA_x-AA)}{Zr(OR)_2(CH_3(CH_2)_{x-2}COO^-)(CH_3COO^-)} + ROH \quad (4)$$

Anhydrolytic condensation:

$$Zr(OR)_2(CH_3(CH_2)_{x-2}COO^-)(CH_3COO^-) + Zr(OR)_3(CH_3(CH_2)_{x-2}COO^-) \rightarrow (CH_3(CH_2)_{x-2}COO^-)(OR)_2Zr - O - Zr(OR)_2(CH_3(CH_2)_{X-2}COO^-) + CH_3COOR \quad (5)$$

$$2Zr(OR)_2(CH_3(CH_2)_{x-2}COO^-)(CH_3COO^-) \rightarrow (CH_3(CH_2)_{x-2}COO^-)(OR)_2Zr - O - Zr(OR)(CH_3(CH_2)_{x-2}COO^-)(CH_3COO^-) + CH_3COOR \quad (6)$$

In the present study, we employed zirconium tetra-propoxide (ZTP, $Zr(OCH_2CH_2CH_3)_4$) 70 wt % in isopropanol (IPA), in the production of a Zr-carboxylic acid ($ZrCA_x$) hybrid (x = total carbon number in the carboxylic acid). ZTP is a common Zr-alkoxide reagent used in a variety of processes, most notably the production of numerous zirconium complexes due to the short residence time and rapid ligand exchange experienced by the Zr-bound propoxide groups at room temperature, which provides an easy route for ligand substitution. In the presence of moisture, ZTP undergoes almost instant hydrolysis forming Zr-hydroxide ($Zr(OH)_4$) gels, however this can usually be prevented by addition of acetic acid (AA), which reversibly attaches to the $Zr^{(IV)}$ center, binding more strongly than propoxide or hydroxyl groups.[43] As a result, ZTP-AA mixtures are stable enough to be added to aqueous solutions indefinitely without hydroxide formation (eq 2). Solvent evaporation during film casting causes ZTP-AA sol−gels to lose acetate groups and undergo Zr-hydroxide formation, with metal-bound propoxides and acetates replaced with hydroxyl groups (eq 3), which in turn undergo polymeric condensation with other Zr species forming an expansive Zr−O−Zr network during calcination.[43−45] Alteration of this system to include carboxylic acid substituted ZTP meant that AA addition was no longer able to provided protection from hydrolysis, addition of water rapidly causing hydroxide gel formation. To overcome these complications, a nonhydrolytic sol−gel process was instead used, in which Zr−O−Zr network formation occurs using a direct condensation reactions between $Zr^{(IV)}$-bound propoxide and carboxylate groups, yielding a carboxylate ester as a coproduct (eqs 4-6).[46,47] Nonhydrolytic sol−gel synthesis routes are relatively poorly explored in comparison to the hydrolytic sol−gel processes. The nonhydrolytic method provides some advantages over traditional hydrolytic routes including the ability to incorporate water sensitive molecules and compounds that contain large hydrophobic groups. However, despite the advantages that the nonhydrolytic sol−gel approach offers to the production of hybrid materials with large organic components, it has only rarely been used in the fabrication of functional surfaces. Overall, monocarboxylated tripropoxide $Zr^{(IV)}$ complexes ($Zr(RCOO)^-(CH_3CH_2CH_2O)_3^-$, where $R{=}CH_3(CH_2)_{x-2}$) were initially prepared, and then mixed with AA to create a transitory bicarboxylated bipropoxide $Zr^{(IV)}$ complex (eq 4), which was able to undergo hetero- and homocondensation (eqs 5 and 6, respectively) and generate an extensive Zr−O−Zr network.

During the characterization of this hybrid, we have particularly focused on the effects the carboxylic acid carbon chain length had on the optical properties, film structures, and dynamic dewetting behavior ($\Delta\theta_{cos}$ and TAs) of the resulting films toward polar (water, as a control) and nonpolar alkane (*n*-hexadecane, *n*-dodecane, and *n*-decane) liquids. Differences in the final dynamic dewetting behavior of the samples are discussed in terms of the surface chemical and physical properties. In this study the minimum achievable $\Delta\theta_{cos}$ and TAs rather than maximum static CAs exhibited by alkane liquids on hybrid film surfaces are considered the most important practical parameters by which the final oleophobic dewetting properties of the material were evaluated.

EXPERIMENTAL SECTION

Materials. Isopropanol (IPA) and stearic acid were purchased from Wako Pure Chemicals, while behenic and lignoceric acids were purchased from Sigma-Aldrich. Zirconium tetra-propoxide 70 wt.% in isopropanol (ZTP), decanoic, lauric, myristic, palmitic, and glacial acetic acids were all purchased from Tokyo Chemical Industries Co., Ltd. All chemicals were used as received without further purification.

Preparation of Zirconium-Carboxylic Acid Hybrid Films. Zirconium-carboxylic acid ($ZrCA_x$; where x = the total carbon number of the carboxylic acid, e.g., 10, 12, 14, 16, 18, 22, or 24) hybrid films were prepared using a sol−gel route by first mixing ZTP (10 mL) with a carboxylic acid (0.02 M) in a dry N_2 atmosphere at 70 °C. When the carboxylic acid was fully dissolved and had been allowed to stir for a further 5 min, the open vial was sealed into a screw cap PTFE vessel and then placed in an oven and maintained at 150 °C overnight. Upon removal from the oven, the vial was placed uncovered in an oven maintained at 80 °C for 6 h to remove excess unligated IPA. Glacial acetic acid (30 μL per milliliter of $ZrCA_x$) was then added to the $ZrCA_X$ with stirring on a hot plate kept at 80 °C; after 2 min, IPA was added at a ratio of 1: 14 by volume ($ZrCA_x$: IPA). The precursor was then instantly spin-cast (at 600 rpm for 5 s followed by 1000 rpm for

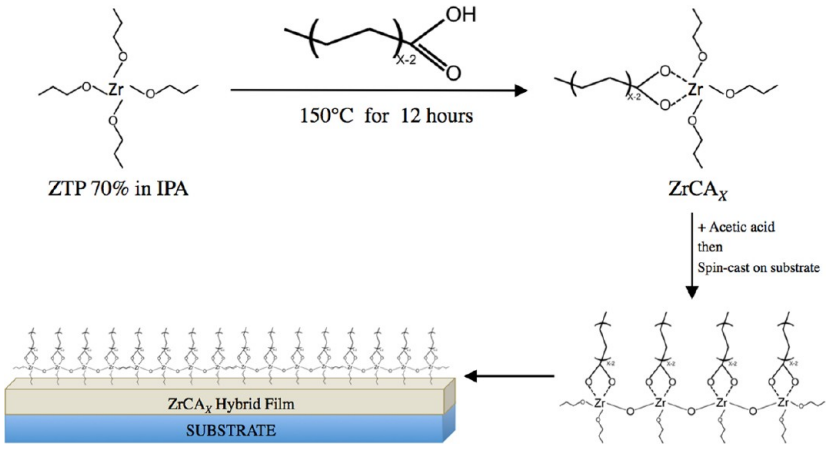

Figure 1. Schematic illustration showing the synthetic steps taken during the formation of ZrCA$_x$ hybrid films.

10 s) onto UV-Ozone cleaned glass slides (28 × 48 mm^2) and single sided Si [100] wafers (15 × 15 mm^2) which had been heated to 80 °C. After coating the samples were dried on a hot plate at 70 °C for 10 min and then cured at 100 °C for 1 h.

Characterization. CA measurements were performed with a Kyowa Interface Science CA-X contact angle instrument. Static CA (θ_S), θ_A and θ_R were collected using Milli-Q water (1 × 10^{-18} Ω/cm), *n*-hexadecane, *n*-dodecane, and *n*-decane at room temperature (~25 °C). θ_S was measured by gently placing a drop of the probe liquid (3 μL) on the horizontal surface. θ_A and θ_R were measured as probe liquid was added and withdrawn from the drop, respectively. CAs were gathered at 5 different locations on each surface. θ_S, θ_A, and θ_R reported are the averages of the 5 values gathered. All measurements were taken at ambient conditions unless otherwise stated, values for each sample were in the range of ±2°. The minimum substrate TA required to set a 5 μL droplet of alkane liquid and 60 μL droplet of water in motion was measured using a Sigma Koki Shot-102 tilt angle stage controlled using a Sigma Koki SGSP-60YAW-OB controller and was taken as an average of at least 5 measurements at different locations on 3 separately prepared samples. The thicknesses of ZrCA$_x$ hybrid films were measured using a stylus profiler (Veeco Dektak 6M). X-ray diffraction (XRD) patterns were taken using a Rigaku RINT 2100 diffractometer with monochromated Fe−K$_\alpha$ radiation over the range 2−16° 2θ. Fourier transform infrared (FT-IR) spectra were attained with an Agilent, Digilab FTS-7000 spectrometer. Final spectra were an average of 256 measurements. The transparencies of the samples were measured using a Varian Cary 5000 UV−vis-NIR spectrometer over a range of 400−800 nm. The morphology of the samples was observed by a Park Systems XE-100 atomic force microscope (AFM) with a Si probe (Park Systems, 910M-NCHR; spring constant = 42 N/m and response frequency of 330 kHz) in noncontact mode, a JEOL JSM-7100F field-emission scanning electron microscope (FE-SEM) and a Kosaka ET-350 stylus profilometer. In the last case, each sample was measured 3 times and the results averaged. The Meyer hardness of the samples was estimated using an instrumented indentation microscope fitted with a Berkovich-type pyramidal diamond indenter (25°).

RESULTS AND DISCUSSION

Film Appearance. ZrCA$_x$ hybrid films were fabricated according to the process illustrated in Figure 1. Stylus profiling estimated the thickness of the hybrid films to be between 410−1110 nm, with the longer alkyl chain ZrCA$_x$ hybrids generally producing a thicker coating due to the higher viscosity of the precursor solutions. All precursor solutions and hybrid films were highly transparent and colorless (Figure 2). UV−vis spectra confirmed that all ZrCA$_{10-24}$ hybrid films cast onto glass slides absorbed on average only 0.95% more light in the visible spectrum (400−800 nm) than the glass slide alone, and showed

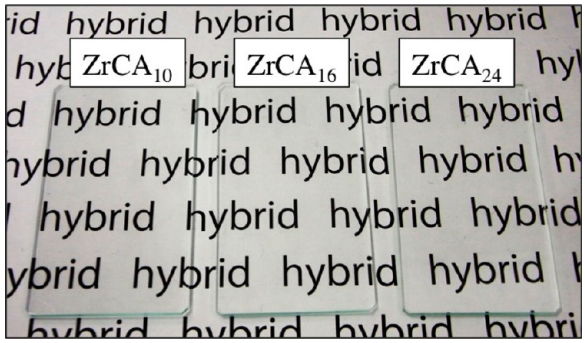

Figure 2. Optical photograph of our ZrCA$_x$ hybrid films on glass slides. All samples were highly transparent and colorless.

no preferential absorption regions (see Figure S-1 in the Supporting Information).

Such excellent transparency was no doubt aided by the highly smooth, and generally defect-free surface of the hybrid films. AFM measurements revealed that the surfaces of all of the cured hybrid films on Si substrates were consistently very smooth, containing no cracks or defects. AFM measurements found that the average root-mean-squared roughness (R_{rms}) of each sample was in the range of 0.208−0.345 nm for a 3 × 3 μm^2 section across the entire range of surfaces (see Table S-2 in Supporting Information for details). In fact, the surfaces were almost as smooth as the bare Si substrate (R_{rms} = 0.2 nm). FE-SEM observation of relatively large areas of the samples revealed smooth, nondescript surfaces and no large-scale defects on any samples of ZrCA$_{10-22}$ with only a small amount of surface contamination by adventitious particles. However, the ZrCA$_{24}$ hybrid surface exhibited some peeling away of small areas of the topmost layer of the film possibly caused by shrinkage during drying (Figure 3) although this did not noticeably reduce the transparency. Stylus profilometry was also used to estimate the R_{rms} of identical samples. The results (see Table S-2 in the Supporting Information for details) revealed that our sample surfaces appeared to be considerably smooth over a large area (about 3 mm stroke). Profilometry R_{rms} values of the surfaces were estimated to be in the range of 9.7 and 54.6 nm with no prominent trend over a range of samples (ZrCA$_{10-24}$). Profilometry results, although larger than those estimated by AFM images, can still be considered very smooth. Such differences in R_{rms} values are likely a result of the striations formed by spin coating, which were detectable only to the

dx.doi.org/10.1021/am302320q | ACS Appl. Mater. Interfaces 2013, 5, 154−163

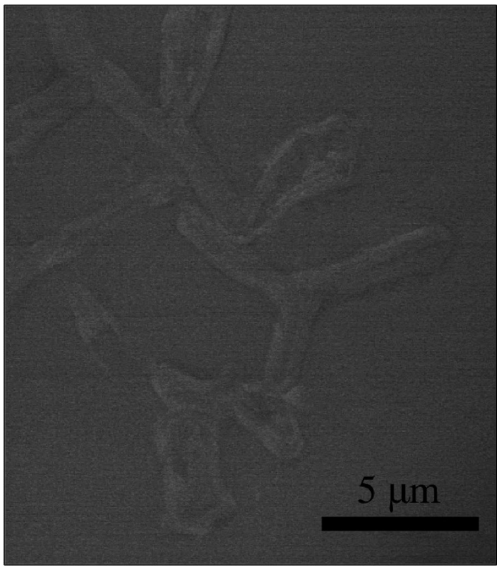

Figure 3. Typical FE-SEM image of a $ZrCA_{24}$ hybrid film surface. Morphologies like this image were partially observed over the entire area of the topmost layer.

larger area measurements and not caused by intrinsic surface roughness.[48]

FT-IR. Figure 4 shows IR transmission spectra of a typical hybrid ($ZrCA_{12}$) film before (a) and after (b) curing at 100 °C for 1 h. The uncured film is shown by spectrum (a) in which significant IR absorption bands can be seen at ~1560 cm^{-1} and ~1450 cm^{-1} that are assigned to the $\nu_{asym}(COO^-)$ and $\nu_{sym}(COO^-)$ stretching vibrations of carboxylic acids, respectively. The other major absorption bands, centered at ~2924 cm^{-1} and ~2855 cm^{-1}, are assigned to $\nu_{asym}(CH_2)$ and $\nu_{sym}(CH_2)$ stretching vibrations, respectively. It is well-known that the position of the $\nu_{asym}(CH_2)$ band is highly dependent on the conformational ordering of the alkyl chains. For instance, the $\nu_{asym}(CH_2)$ absorption for highly packed and therefore solid-like alkyl-chains is generally centered below 2920 cm^{-1}, whereas alkyl chains that have a lower packing density and therefore a more flexible and liquid-like nature typically absorbs at higher wavenumbers (see Figure S-3 in the Supporting Information for peak positions). The $\nu_{asym}(CH_2)$ peak positions gradually moved from 2925.5 cm^{-1} to 2919.5 cm^{-1} as the alkyl chain length of the hybrid film increased from $ZrCA_{10}$ to $ZrCA_{24}$, representing a significant change to the physical nature of the hybrid films from liquid-like to solid-like as the alkyl chain length increases. This change was attributed to the longer alkyl chains in the films causing greater mutual inhibition of movement by colliding more with neighboring chains, resulting in a more solidlike surface. The effect of this physical change on film dewettability is further discussed later. In addition, this spectrum shows peaks at around 1740 cm^{-1} and 1176 cm^{-1} corresponding to the ν(C═O) and ν(CO) vibrations of an ester, respectively. A coproduct of nonhydrolytic condensation, the presence of esters in the films is evidence that Zr−O−Zr bond formation had occurred. Furthermore, the low nucleophilicity of esters compared to water reduces the chance of any Zr−O−Zr bond breaking cleavage reactions, often seen in hydrolytic condensation reactions (eqs 5 and 6).

After curing of the films at 100 °C for 1 h, the two ester absorption bands completely vanish, while the former four bands still remained, as shown in spectrum b. This implies that the esters were likely only acting as solvents, and that all of the carboxylic acids remained bound to the Zr centers in the cured films. Additionally, in both spectra the characteristic peaks of Zr−O−Zr bonds at ~460 cm^{-1} and Zr−O bonds at 653 cm^{-1} and 618 cm^{-1} were prominent. Significantly, the absorption intensities corresponding to the Zr−O−Zr bonds increased relative to those of the Zr−O bonds during curing, (a) to (b), indicating promotion of Zr−O−Zr cross-linking in the matrix during curing and not only in the sol−gel. The increased Zr−O−Zr network growth resulted in a film that upon application of IPA, ester solvents or short chain alkane liquids remained solid, resisting resolvation.

Film Structures. XRD revealed that some of the $ZrCA_X$ hybrid films possess multilayered nanostructures before curing, which was confirmed by the presence of strong, sharp, and regular diffraction peaks (Figure 5a). Zr phosphate and Zr phosphonates are well-known to possess layered structures;[49−51] however highly lamella Zr-carboxylic acid hybrids are previously unknown. Such materials are more commonly associated with mesoporous structures, which have long been exploited in the production of high surface area and functional ZrO_2 materials. Of the $ZrCA_X$ hybrid films produced, only those with longer chain alkyl groups ($ZrCA_{18,\ 22,\ and\ 24}$) demonstrated the lamella structure (see Figure S-4 in the Supporting Information). Subsequent *d*-spacing calculations gave the interlayer distance as 29.5, 30.4, and 32.7 Å, respectively. The *d*-spacings are much smaller than might be expected for bilayers because straight chain C_{18}, C_{22}, and C_{24} carboxylic acid groups theoretically measure 22.5, 27.5, and 30.0 Å, respectively, when fully extended in an all-trans configuration. Considering the layer thicknesses and the solidlike (closely packed) nature of these long alkyl chain-containing groups (see Figure S-3 in the Supporting Information), the interlayer region of the hybrid was assumed to consist of interdigitated monomolecular alkyl chains.[52−54]

As mentioned in the previous section, the $ZrCA_x$ films became more solid and stable as a result of Zr−O−Zr bonding after curing at 100 °C for 1 h. However, the well-ordered periodic lamellar structures of the film distorted significantly during the 60 min thermal treatment, even at 60 °C, and were completely collapsed at 100 °C, as shown in Figure 5. In addition, according to the FT-IR data, the thermal treatment effectively promoted the anhydrolytic condensation reactions simultaneously in the Zr matrices. However, considering the actual hardness data of the samples, at present their mechanical properties are insufficient for many practical applications. Even after thermal treatment, area sensing indentation tests revealed the Meyer hardness of the film to be ~200 MPa. XPS investigations provided an explanation of this low hardness revealing that a considerable amount of carbon (71.7−85.9 at %) is present in the topmost region of the sample close to the surface (data not shown), leading to the poor scratch resistance and surface hardness observed. However, adhesion between our hybrid films and the glass slides was very stable even after cross-cutting and boiling water (90 °C) treatment for 45 min. No peeling of the films was observed after ten repetitions of a standard 3M Scotch-tape peeling test.[55,56]

In spite of our hybrid films having such excellent adhesion, the dynamic oleophobicity of the surfaces was unstable upon submersion in hot water (70 °C, see Figure S-5 in the Supporting Information). *n*-Hexadecane displayed small decreases in θ_S and θ_A, but θ_R decreased sharply after only 2

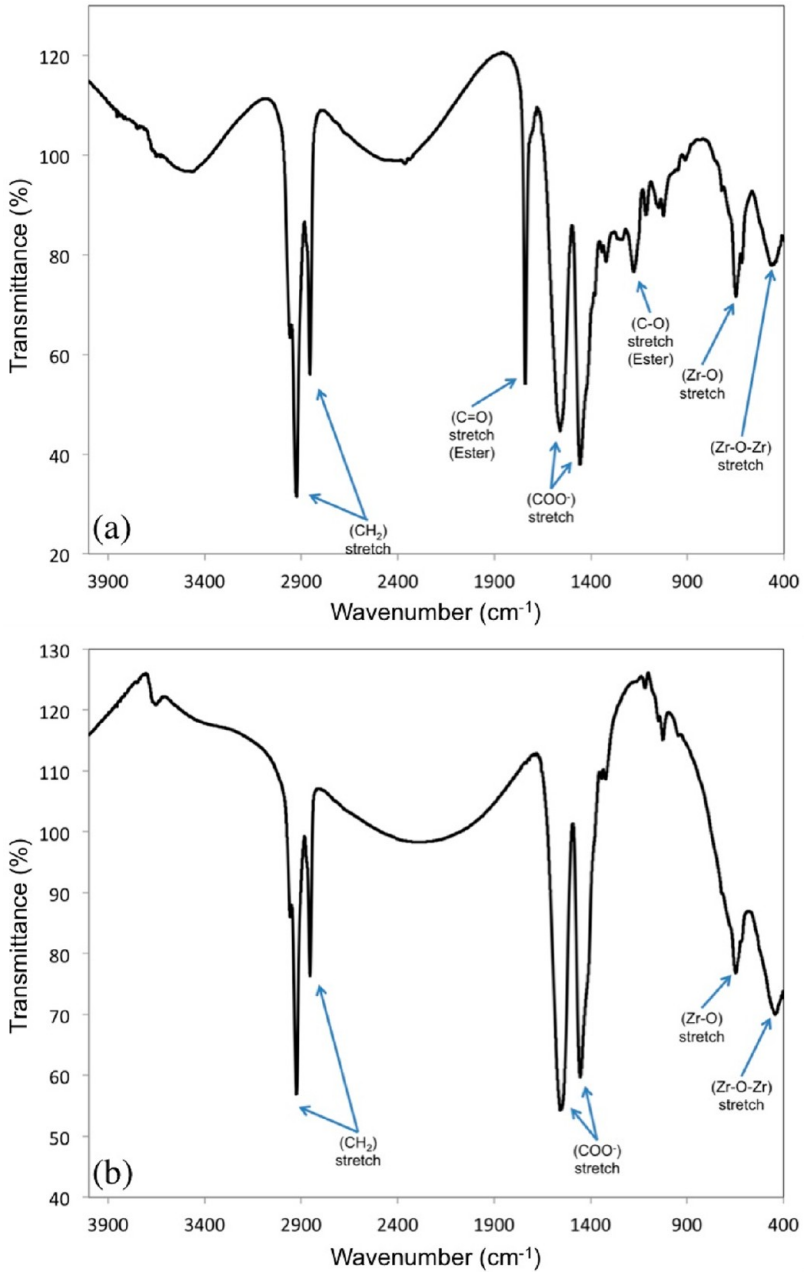

Figure 4. FT-IR spectra of a typical hybrid ($ZrCA_{12}$) film (a) before and (b) after curing for at 100 °C for 1 h.

min submersion, becoming completely wetted after 5 min submersion.

Film Dewettability. Figure 6 clearly indicates that our $ZrCA_x$ hybrid films (x = 10−24) were all hydrophobic but oleophilic, displaying low static CAs (<30°) for alkane probe liquids, with little variation across the full range of hybrid films. As a result of the decreasing surface tension, the profile of the liquid droplets and the resulting static CAs decreases from water to *n*-decane. However, despite such low static CAs, in a dynamic situation the resulting surfaces exhibited excellent dewettability (Figure 7 and Table 1), with small volume alkane liquid droplets sliding off the surface at very low TAs (see Movie S-6 in the Supporting Information). The $ZrCA_{14}$ surface possessed the best dynamic dewettability properties, exhibiting $\Delta\theta_{cos}$ of 0.028, 0.015, and 0.004; and TAs of 6.25, 4.2, and 2.95°, for *n*-hexadecane, *n*-dodecane, and *n*-decane, respectively. This is comparable to conventional flat perfluorinated surfaces (e.g., TA ∼ 5° for 5 μL of *n*-hexadecane on Teflon AF1600) and nonflat perfluorinated superoleophobic surfaces with static CAs >160° (e.g., TA = 5.3° for 5 μL for *n*-decane on nanofilament surface).[2]

Such unusual dynamic dewetting behavior of our $ZrCA_x$ film surfaces toward alkane liquids cannot be explained simply by the different chemistry of the surface functional groups, because they are all similar carboxylic acids with straight alkyl chains. Additionally, the smooth surfaces and film structures (lamella or amorphous) are expected to have little if any influence on the dewettability. Thus, we believe that the physical properties (solidlike or liquidlike) of the alkyl chains in the film surface must be responsible for the differences in the observed dynamic dewettability. As described in the previous section, FT-IR spectroscopy (see Figure S-3 in the Supporting Information) displays a clear shift in the position of the $\nu_{asym}(CH_2)$ vibration to lower wavenumbers as the length of the alkyl chain increases.

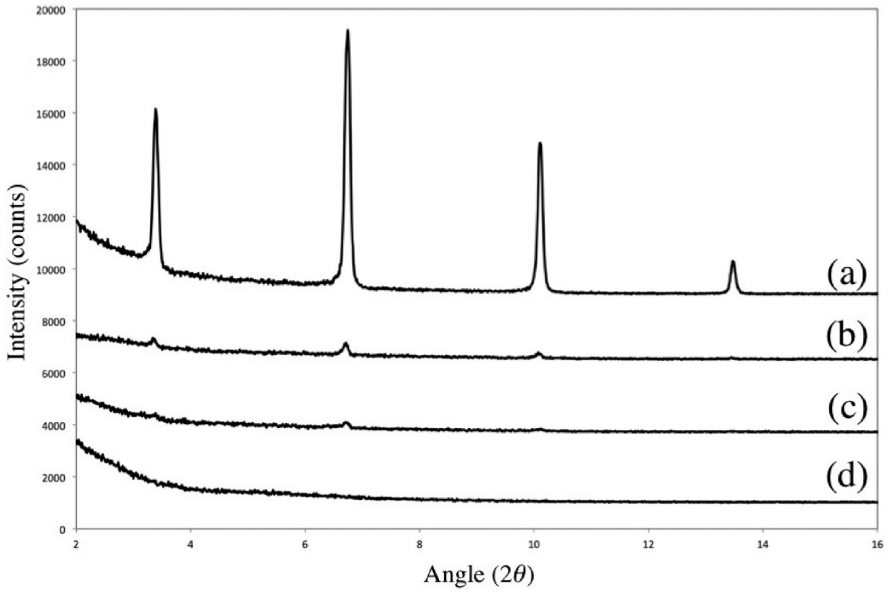

Figure 5. XRD trace of the $ZrCA_{24}$ hybrid film: (a) initial, and cured for 1 h at (b) 60, (c) 80, and (d) 100 °C, respectively. Initial hybrid film a demonstrates a layered structure with an initial *d*-spacing of 32.7 Å (1.1 μm thick).

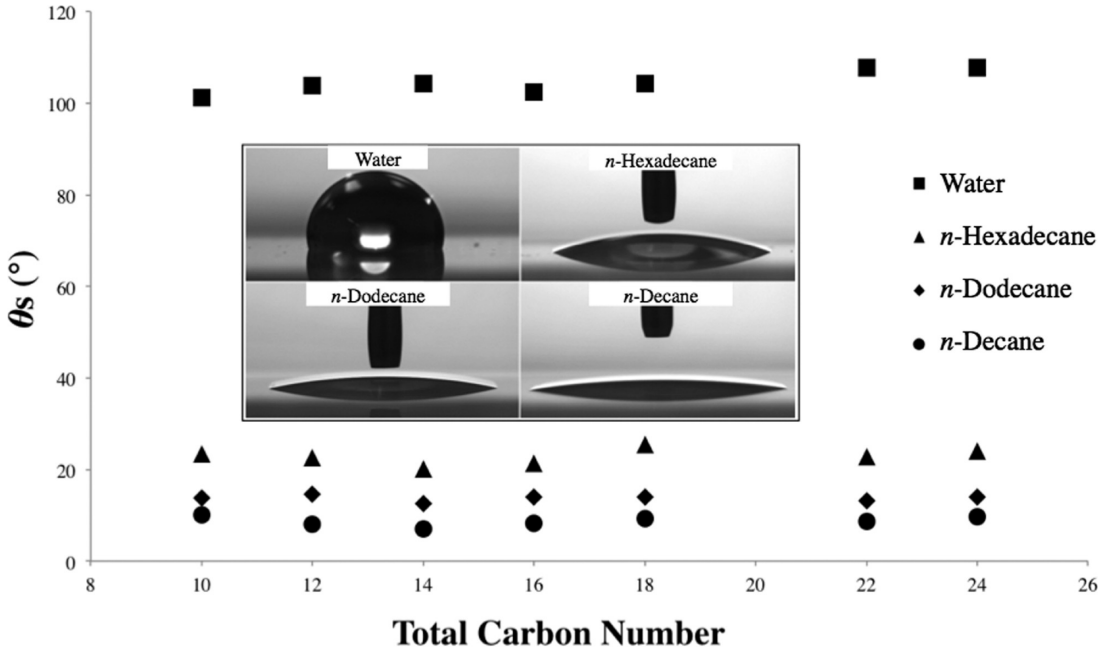

Figure 6. Static CAs versus total carbon number of the carboxylic acids for the 4 probe liquids.

Although we cannot directly estimate the physical mobility of the surface-tethered alkyl chains by FT-IR, it suggests that the alkyl chain mobility was probably inhibited by mutual interaction between neighboring alkyl chains, which became greater as the chain length increased. Therefore, the overall mobility of the alkyl chains is, unsurprisingly, decreased as the chain length increased, enhancing the solidlike nature of the surface. In addition, surface defects (for example, the $ZrCA_{24}$ hybrid film surface shown in Figure 3) may also contribute to CA hysteresis and help induce the "pinning effect" of the alkane droplets to the surface. These both create a greater resistance to motion of the advancing and receding contact lines. Hence the dewettability of the longer chain hybrid films, in particular $ZrCA_{22,\ 24}$ films, toward alkane liquids became worse. On the other hand, when the carbon number of the alkyl chain was as small as 16, greater freedom of the alkyl chains may have allowed the surface to exhibit significant liquid-like behavior. The shorter alkyl chains provided less resistance to the motion of contact lines of the probe liquids, resulting in lower CA hysteresis and substrate TAs. However, this effect became limited for $ZrCA_x$ hybrid films where $x < 14$, which demonstrated a reduction in the average surface dewettability for all alkane probe liquids.

To further validate our proposed mechanism, changes in dynamic dewetting behavior of *n*-hexadecane on $ZrCA_x$ hybrid films before and after heating to 70 °C were studied. At elevated temperatures mutual interactions between neighboring alkyl chains may decrease and in doing so even the more

dx.doi.org/10.1021/am302320q | *ACS Appl. Mater. Interfaces* 2013, 5, 154−163

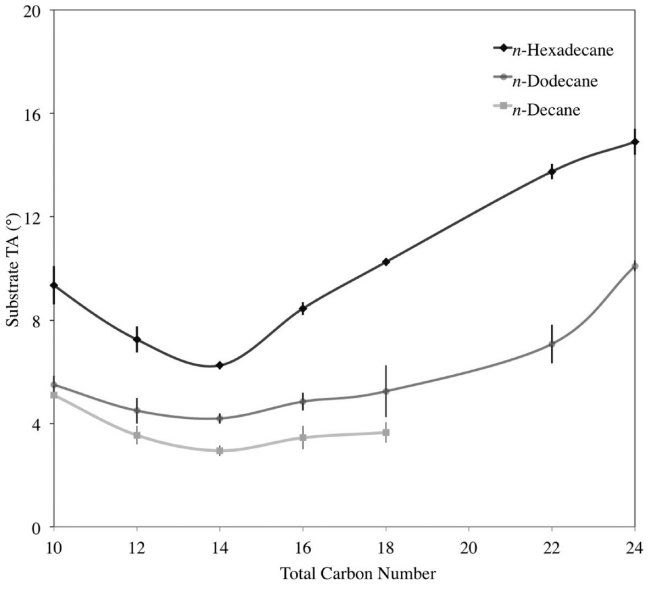

Figure 7. Minimum substrate TAs required to set a 5 μL droplet of *n*-hexadecane, *n*-dodecane, or *n*-decane in motion. This figure shows that $ZrCA_{14}$ possesses the best dynamic dewettability for these probe liquids. (*n*-decane droplets did not completely dewet from $ZrCA_{22\ and\ 24}$).

solidlike surfaces (carbon number >14) are expected to become increasingly liquid-like. In fact, as Figure 8 clearly indicates, the dynamic dewettability of our $ZrCA_x$ hybrid films toward alkane liquids is strongly affected by substrate temperature. At room temperature, for example, $ZrCA_{14}$ films exhibited the lowest $\Delta\theta_{cos}$ (0.028), whereas $ZrCA_{24}$ film showed the highest (0.078), with $\Delta\theta_{cos}$ steadily increasing as the alkyl chain length increases. On the other hand, at 70 °C $\Delta\theta_{cos}$ reduced significantly when the total carbon number was over 14, becoming virtually constant and independent of the total carbon number. Therefore, simply increasing the temperature of the substrate can be concluded to impart a more liquidlike character to the surfaces. Such thermosensitive dynamic oleophobicity has recently been reported by the authors for poly(dimethylsiloxane) (PDMS) brush film-covered surfaces.[36] These results therefore provide further evidence that the dynamic oleophobicity can be governed by controlling the physical nature (solidlike or liquidlike) of functional groups in the surface-tethered molecules.

It is well-known that the dewettability of perfluorinated coatings typically becomes worse as the surface tension of the probe liquids decrease; however the opposite phenomenon was observed for the $ZrCA_x$ family of materials. Lower surface tension probe liquids were able to easily slide off our $ZrCA_x$ surfaces, particularly $ZrCA_{14}$, at much lower TAs than water. As the mutual affinity of the surface and the probe liquid increases, the minimum required substrate TA decreases, indicating better dynamic dewettability. The solubility of alkyl chains with alkane liquids must also be taken into account because it will result in the further enhancement of the liquidlike property of the surface bound alkyl chains. The results point to the formation of a "blended interface" between the probe liquid and the surface tethered alkyl chains, similar but not as extensive as that previously postulated by the authors.[36,37] As a result, the lower carbon number probe liquids are capable of greater solvent interactions than those with higher carbon numbers (in the present case *n*-decane and *n*-hexadecane, respectively). The consequence was lower static CAs, $\Delta\theta_{cos}$, and TAs for *n*-decane rather than *n*-dodecane or *n*-hexadecane. Our results emphasize the applicability of this material, as well as highlighting that surface perfluorination is not always the best option when creating highly dewettable materials, especially for low surface tension liquids.

CONCLUSIONS

A facile and reproducible strategy to prepare novel zirconium-based hybrid films using a nonhydrolytic sol−gel process was presented. Monocarboxylic acid substituted zirconium tripropoxide precursors, $Zr(CH_3(CH_2)_2O)_3(CH_3(CH_2)_{x-2}COO)$ ($ZrCA_X$) where x = 10, 12, 14, 16, 18, 22, 24, were first synthesized and then spin-cast into uniform hybrid films, undergoing direct condensation in the anhydrous mixture to form a Zr−O−Zr network with the aid of acetic acid. After curing all films were highly transparent, smooth and stable against resolvation, with an average film thickness of 410 − 1100 nm. Some of the samples ($ZrCA_{x\geq 18}$) displayed well-ordered lamella structures, greatly depending on both alkyl chain length of carboxylic acids and curing conditions. Dynamic contact angle measurements confirmed that our film surfaces exhibited unusual dynamic dewetting behavior toward three low surface tension alkane liquids (*n*-hexadecane, *n*-dodecane, and *n*-decane) even though the films displayed oleophilic tendencies in static situations. We suspect this unusual wetting behavior is related to both physical (solidlike or liquidlike) properties of the alkyl chain assemblies and the mutual affinity of the surface and the probe liquids. The longer alkyl chains ($x \geq 18$) not only caused the formation of self-assembled, well-ordered nanostructures but also imparted solid-like properties to the surfaces and as such provided resistance to the motion of

Table 1. θ_A/θ_R, $\Delta\theta_{cos}$, and Substrate TAs for the 4 Probe Liquids on $ZrCA_{10\text{-}24}$ Hybrid Films

	probe liquid (surface tension)											
	n-hexadecane (26.6 mN/m)			*n*-dodecane (24.5 mN/m)			*n*-decane (23.8 mN/m)			water (72 mN/m)		
sample name	θ_A/θ_R (deg)	$\Delta\theta_{cos}$	TA (deg)	θ_A/θ_R (deg)	$\Delta\theta_{cos}$	TA (deg)	θ_A/θ_R (°)	$\Delta\theta_{cos}$	TA (deg)	θ_A/θ_R (deg)	$\Delta\theta_{cos}$	TA (deg)[a]
$ZrCA_{10}$	24.5/16.7	0.048	9.35	14.8/8.6	0.022	5.50	10.5/6.5	0.010	5.10	107/55.3	0.857	63.0
$ZrCA_{12}$	22.7/17.3	0.032	7.25	14.8/10.4	0.017	4.50	8.3/5.5	0.006	3.55	109/41.7	1.064	62.0
$ZrCA_{14}$	20.7/15.5	0.028	6.25	13.8/9.6	0.015	4.20	7.5/5.4	0.004	2.95	109/13.2	1.294	61.5
$ZrCA_{16}$	21.9/16.0	0.033	8.45	14.5/9.9	0.016	4.85	8.8/5.0	0.008	3.45	108/15.0	1.274	61.0
$ZrCA_{18}$	25.7/16.4	0.058	10.25	14.8/8.2	0.023	5.25	10.4/5.8	0.011	3.65	111/16.2	1.317	36.0
$ZrCA_{22}$	23.1/11.7	0.059	13.75	14.2/7.2	0.022	7.08	N/A	N/A	N/A	113/92.9	0.356	19.5
$ZrCA_{24}$	25.6/11.6	0.078	14.90	14.9/4.9	0.030	10.10	N/A	N/A	N/A	117/96.9	0.329	18.5

[a]60 μL droplets of water were used during TA measurements.

dx.doi.org/10.1021/am302320q | ACS Appl. Mater. Interfaces 2013, 5, 154−163

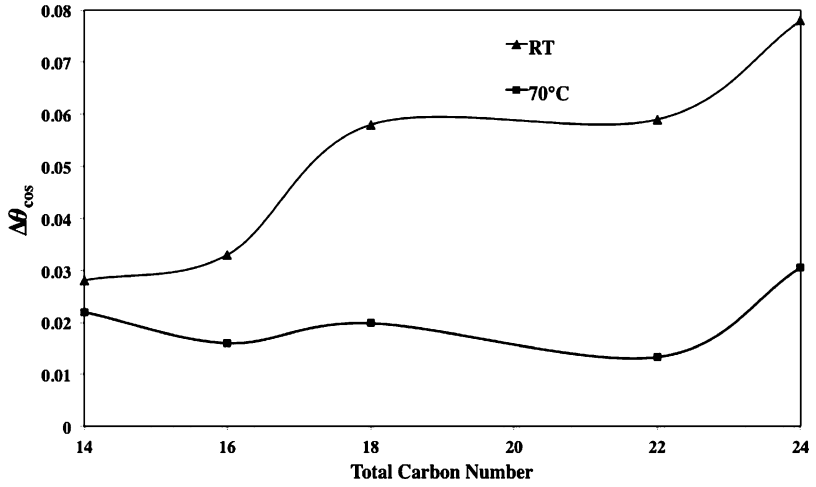

Figure 8. Changes in $\Delta\theta_{cos}$ for *n*-hexadecane on $ZrCA_x$ hybrid films before and after heating at 70 °C. When the total carbon number was greater than 14, $\Delta\theta_{cos}$ decreased markedly by heating to 70 °C and became virtually constant, independent of total carbon number.

contact lines of the probe liquids, resulting in a decrease of dynamic oleophobicity. Among the seven $ZrCA_x$ films fabricated in the present study, the $ZrCA_{14}$ film surface was found to demonstrate the lowest contact angle hysteresis and tilt angles for all probe liquids (~4° and ~6° for *n*-hexadecane, respectively) because of the liquidlike nature of the alkyl chains at the surface. In addition, increasing the temperature of the substrate to 70 °C also weakened interactions between neighboring alkyl chains, resulting in a significant increase of dynamic oleophobicity of longer alkyl chain (carbon number >14)-derived hybrid films. CA measurements made using *n*-hexadecane demonstrated that at elevated temperatures the alkyl chain length had little or no effect on the dynamic dewettability of the films. These results provided further evidence that the physical nature (solidlike or liquidlike) of the surface-tethered alkyl chains is the most defining factor in the successful control of dynamic oleophobicity for smooth surfaces. Such excellent dynamic dewetting properties of our best sample are comparable to Teflon AF1600 and other superoleophobic perfluorinated surfaces with static contact angles >160° reported thus far.

These results provide important insight into the varied applicability of our new hybrid materials for expanding and improving the current catalogue of oleophobic/superoleophobic coatings, and emphasize that conventional surface perfluorination is not always the best way to design highly dewettable surfaces for low surface tension liquids. We can expect that our new findings offer an alternative approach for the future production of oleophobic coatings without relying on conventional surface structuring and perfluorination.

■ ASSOCIATED CONTENT

Supporting Information

Further information on the transparency, surface roughness, FT-IR peak positions (before and after curing), X-ray diffraction patterns, and hydrolytic stability; as well as a movie showing *n*-dodecane dewetting a $ZrCA_{14}$ hybrid films surface. This material is available free of charge via the Internet at http://pubs.acs.org/.

■ AUTHOR INFORMATION

Corresponding Author

*E-mail: a.hozumi@aist.go.jp.

Notes

The authors declare no competing financial interest.

■ ACKNOWLEDGMENTS

We thank Dr. Tatsuya Miyajima, Dr. Tatsuo Kimura, and Dr. Takeshi Kusumori of AIST for their assistance with the hardness testing, XRD, and profilometry, respectively. This work was partially supported by a Grant-in-Aid for Scientific Research on Innovative Areas (A.H. and C.U.; 24120005) and Research Activity Start-up (C.U.; 23850020) of The Ministry of Education, Culture, Sports, Science, and Technology (MEXT), Japan.

■ REFERENCES

(1) Chen, Y.; Zhang, Y.; Shi, L.; Li, J.; Xin, Y.; Yang, T.; Guo, Z. *App. Phys. Lett.* **2012**, *101*, 033701−033701−4.
(2) Zhang, J. P.; Seeger, S. *Angew. Chem., Int. Ed.* **2011**, *50*, 6652−6656.
(3) Jung, Y. C.; Bhushan, B. *ACS Nano* **2009**, *3*, 4155−4163.
(4) Li, S. M.; Zhou, S. Z.; Liu, J. H. *Acta Phys. Chim. Sin.* **2009**, *25*, 2581−2589.
(5) Barkhudarov, P. M.; Shah, P. B.; Watkins, E. B.; Doshi, D. A.; Brinker, C. J.; Majewski, J. *Corros. Sci.* **2008**, *50*, 897−902.
(6) Michalski, M. C.; Desobry, S.; Hardy, J. *Crit. Rev. Food Sci.* **1997**, *37*, 591−619.
(7) Barish, J. A.; Goddard, J. M. *J. Food Sci.* **2011**, *76*, E586−E591.
(8) Wong, T. S.; Kang, S. H.; Tang, S. K. Y.; Smythe, E.; Hatton, B. D.; Grinthal, A.; Aizenberg, J. *Nature* **2011**, *477*, 443−447.
(9) Tuteja, A.; Choi, W.; Ma, M.; Mabry, J. M.; Mazzella, S. A.; Rutledge, G. C.; McKinley, G. H.; Cohen, R. E. *Science* **2007**, *318*, 1618−1622.
(10) Quéré, D.; Reyssat, M. *Philos. Trans. R. Soc. London, Ser. A* **2008**, *366*, 1539−1556.
(11) Wei, P. J.; Chen, S. C.; Lin, J. F. *Langmuir* **2009**, *25*, 1526−1528.
(12) Lin, L.; Cai, Y.; Wang, X.; Ding, B.; Yuc, J.; Wang, M. *Nanoscale* **2011**, *3*, 1258−1262.
(13) Hozumi, A.; McCarthy, T. J. *Langmuir* **2010**, *26*, 2567−2573.
(14) Wier, K. A.; Gao, L. C.; McCarthy, T. J. *Langmuir* **2006**, *22*, 4914−4916.
(15) Kawasaki, K. J. *Colloid Sci.* **1960**, *15*, 402−407.
(16) Furmidge, C. G. J. *Colloid Sci.* **1962**, *17*, 309−324.
(17) Erbil, H. Y.; Demirel, A. L.; Avci, Y.; Mert, O. *Science* **2003**, *299*, 1377−1380.

(18) Lau, K. K. S.; Bico, J.; Teo, K. B. K; Chhowalla, M.; Amaratunga, G. A. J.; Milne, W. I.; McKinley, G. H.; Gleason, K. K. *Nano Lett.* **2003**, *3*, 1701−1705.
(19) Zhai, L.; Cebeci, F. C.; Cohen, R. E.; Rubner, M. F. *Nano Lett.* **2004**, *4*, 1349−1353.
(20) Nakajima, A.; Fujishima, A.; Hashimoto, K.; Watanabe, T. *Adv. Mater.* **1999**, *11*, 1365−1368.
(21) Quéré, D. *Rep. Prog. Phys.* **2005**, *68*, 2495−2532.
(22) Bhushan, B.; Jung, Y. C. *Nanotechnology* **2006**, *17*, 2758−2772.
(23) Tuteja, A.; Choi, W.; Mabry, J. M.; McKinley, G. H.; Cohen, R. E. *P. Natl. Acad. Sci. USA.* **2008**, *105*, 18200−18205.
(24) Grainger, D. W.; Stewart, C. W.; *Fluorinated Coatings and Films: Motivation and Significance*; ACS Symposium Series; American Chemical Society: Washington, D.C., 2001; Vol. *787*, pp 1−14.
(25) Deng, X.; Mammem, L.; Butt, H. J.; Vollmer, D. *Science* **2012**, *335*, 67−70.
(26) Zushi, Y.; Hogarh, J. N.; Masunaga, S. *Clean Technol. Environ. Policy* **2011**, *14*, 9−20.
(27) Lindstrom, A. B.; Strynar, M. J.; Libelo, E. L. *Environ. Sci. Technol.* **2011**, *45*, 7954−7961.
(28) Zaggia, A.; Ameduri, B. *Curr. Opin. Colloid Interface Sci.* **2012**, *17*, 188−195.
(29) Chen, W.; Fadeev, A. Y.; Hsieh, M. C.; Oner, D.; Youngblood, J.; McCarthy, T. J. *Langmuir* **1999**, *15*, 3395−3399.
(30) Fadeev, A. Y.; McCarthy, T. J. *Langmuir* **1999**, *15*, 7238−7243.
(31) Hozumi, A.; Cheng, D. F.; Yagihashi, M. *J. Colloid Interface Sci.* **2011**, *353*, 582−587.
(32) Fadeev, A. Y.; McCarthy, T. J. *Langmuir* **1999**, *15*, 3759−3766.
(33) Youngblood, J. P.; McCarthy, T. J. *Macromolecules* **1999**, *32*, 6800−6806.
(34) Fadeev, A. Y.; McCarthy, T. J. *Langmuir.* **2000**, *16*, 7268−7274.
(35) Krumpfer, J. W.; McCarthy, T. J. *Faraday Discuss.* **2010**, *146*, 103−110.
(36) Cheng, D. F.; Urata, C.; Yagihashi, M.; Hozumi, A. *Angew. Chem., Int. Ed.* **2012**, *51*, 2956−2959.
(37) Cheng, D. F.; Urata, C.; Masheder, B.; Hozumi, A. *J. Am. Chem. Soc.* **2012**, *134*, 10191−10199.
(38) Fadeev, A. Y.; McCarthy, T. J. *J. Am. Chem. Soc.* **1999**, *121*, 12184−12185.
(39) Urata, C.; Cheng, D. F.; Masheder, B.; Hozumi, A. *RSC Adv.* **2012**, *2*, 9805−9808.
(40) Xiu, Y.; Hess, D. W.; Wong, C. R. *J. Colloid Interface Sci.* **2008**, *326*, 465−470.
(41) Gonzalez-Martin, M. L.; Labajos-Broncano, L.; Janczuk, B.; Bruque, J. M. *J. Mat. Sci.* **1999**, *34*, 5923−5926.
(42) Di Maggio, R.; Fambri, L.; Guerriero, A. *Chem. Mater.* **1998**, *10*, 1777−1784.
(43) Filiaggi, M. J.; Pilliar, R. M.; Yakubovich, R.; Shapiro, G. *J. Biomed. Mater. Res.* **1996**, *33*, 225−238.
(44) Nabavi, M.; Doeuff, S.; Sanchez, C.; Livage, J. *J. Non-Cryst. Solids* **1990**, *121*, 31−34.
(45) Pascual, R.; Sayer, M.; Kumar, C. V. R. V.; Zou, L. C. *J. Appl. Phys.* **1991**, *70*, 2348−2352.
(46) Jansen, M.; Guenther, E. *Chem. Mater.* **1995**, *11*, 2110−2114.
(47) Mutin, P. H.; Vioux, A. *Chem. Mater.* **2009**, *21*, 582−596.
(48) Kozuka, H.; Takenaka, S.; Kimura, S. *Scripta Mater.* **2001**, *44*, 1807−1811.
(49) Kim, J. D.; Mori, T.; Honma, I. *J. Power Sources* **2007**, *172*, 694−697.
(50) Alberti, G.; Casciola, M. *Solid State Ionics* **1997**, *97*, 177−186.
(51) Byrd, H.; Whipps, S.; Pike, J. K.; Ma, J.; Nagler, S. E.; Talham, D. R. *J. Am. Chem. Soc.* **1994**, *116*, 295−301.
(52) Fujii, K.; Fujita, T.; Iyi, N.; Kodama, H.; Kitamura, K.; Yamagishi, A. *J. Mater. Sci. Lett.* **2003**, *22*, 1459−1461.
(53) Shimojima, A.; Sugahara, Y.; Kuroda, K. *B. Chem. Soc. JPN.* **1997**, *70*, 2847−2853.
(54) Shimojima, A.; Kuroda, K. *Langmuir* **2002**, *18*, 1144−1149.
(55) Spiegel, A.; Bruenger, W. H.; Dzionk, C.; Schmuki, P. *Microelectron. Eng.* **2003**, *67*−*68*, 175−181.
(56) Hidber, P. C.; Helbig, W.; Kim, E.; Whitesides, G. M. *Langmuir* **1996**, *12*, 1375−1380.